Geophysical Research Letters

RESEARCH LETTER
10.1029/2022GL100745

Key Points:

- The seasonal shift in Arctic amplification (AA) annual maximum into winter is more evident than that of Arctic precipitation in the 21st century
- Decomposition shows that uncertainty in Arctic climate change projections is dominated by model differences and also shifts into winter
- Unlike Arctic temperature, precipitation, and sea-ice area, AA is not substantially affected by scenario uncertainty

Supporting Information:

Supporting Information may be found in the online version of this article.

Correspondence to:

Y.-T. Wu,
youtingw11@gmail.com

Citation:

Wu, Y.-T., Liang, Y.-C., Kuo, Y.-N., Lehner, F., Previdi, M., Polvani, L. M., et al. (2023). Exploiting SMILEs and the CMIP5 archive to understand Arctic climate change seasonality and uncertainty. *Geophysical Research Letters*, *50*, e2022GL100745. https://doi.org/10.1029/2022GL100745

Received 9 AUG 2022
Accepted 22 DEC 2022

Exploiting SMILEs and the CMIP5 Archive to Understand Arctic Climate Change Seasonality and Uncertainty

You-Ting Wu[1], Yu-Chiao Liang[1,2], Yan-Ning Kuo[3], Flavio Lehner[3,4], Michael Previdi[2], Lorenzo M. Polvani[2,5,6], Min-Hui Lo[1], and Chia-Wei Lan[1]

[1]Department of Atmospheric Sciences, National Taiwan University, Taipei, Taiwan, [2]Lamont-Doherty Earth Observatory, Columbia University, Palisades, NY, USA, [3]Department of Earth and Atmospheric Sciences, Cornell University, Ithaca, NY, USA, [4]Climate and Global Dynamics Laboratory, National Center for Atmospheric Research, Boulder, CO, USA, [5]Department of Earth and Environmental Sciences, Columbia University, New York, NY, USA, [6]Department of Applied Physics and Applied Mathematics, Columbia University, New York, NY, USA

Abstract Arctic Amplification (AA) exhibits a distinct seasonal dependence; it is weakest in boreal summer and strongest in winter. Here, we analyze simulations from single-model initial-condition large ensembles and Coupled Model Intercomparison Project Phase 5 to decipher the seasonal evolution of Arctic climate change. Models agree that the annual maximum AA shifts from autumn into winter over the 21st century, accompanied by similar shifts in sea-ice loss and surface turbulent heat fluxes, whereas the maximum precipitation shifts only into late autumn. However, the exact seasonal timing and magnitude of these shifts are highly uncertain. Decomposing the uncertainty into model structural differences, emission scenarios, and internal variability reveals that model differences dominate the total uncertainty, which also undergo autumn-to-winter shifts. We also find that the scenario uncertainty is unimportant for projections of AA. These results highlight that understanding model differences is critical to reducing uncertainty in projected Arctic climate change.

Plain Language Summary The Arctic climate has experienced considerably greater warming compared with the global mean in recent decades in response to increasing amounts of atmospheric greenhouse gases. This phenomenon is called Arctic amplification (AA), and global climate models predict that it will continue in the future. AA exhibits a distinct seasonal dependence: it is weakest in summer and strongest in winter of the Northern Hemisphere. Here, we find that global climate models predict that the annual maximum AA (i.e., the greatest difference between Arctic and global temperatures) shifts from autumn into winter over the 21st century. However, this seasonal shift can differ considerably between models in terms of its strength and the number of corresponding months, indicating that substantial uncertainty exists. Our findings highlight the importance of identifying model structural uncertainty in projections of Arctic climate change.

1. Introduction

Arctic amplification (AA) is a phenomenon of anthropogenic climate change in which the near-surface air temperatures (SATs) in the Arctic increase more rapidly than do those in the rest of the globe (Chylek et al., 2022; Holland & Bitz, 2003; Manabe & Wetherald, 1975; Pithan & Mauritsen, 2014; Previdi et al., 2021; Rantanen et al., 2022). AA has a distinct seasonal dependence: it is nonexistent during boreal summer, emerges in early autumn, and is greatest in late autumn and winter (Boeke & Taylor, 2018; Chung et al., 2021; Goosse et al., 2018; Previdi et al., 2021; Sejas et al., 2014; P. C. Taylor et al., 2021). Several studies have indicated that AA seasonality may change in response to increasing levels of greenhouse gases forcing (Hahn et al., 2022; Holland & Landrum, 2021; Liang, Polvani, & Mitevski, 2022). For example, a recent study that performed a suite of experiments involving an abrupt increase in carbon dioxide (CO_2) demonstrated that the maximum AA shifts from autumn to winter as CO_2 forcing increases; this shift was attributed to an accompanying seasonal shift in sea-ice area (SIA) loss and subsequent surface turbulent heat fluxes (THFs) from the ocean into the atmosphere (Liang, Polvani, & Mitevski, 2022). In addition, the sea-ice effective heat capacity (i.e., the thermal inertia of the sea-ice layer) was shown to contribute to this shift in the Arctic warming maximum from autumn to winter (Hahn et al., 2022). Similar seasonal shifting in Arctic warming has also been observed in Coupled Model Intercomparison Project (CMIP) projections under Representative Concentration Pathway (RCP) or Shared Socioeconomic

Pathway (SSP) scenarios, but the models differ considerably in terms of both the warming amplitude and the number of months that the maximum AA shifts from autumn into winter (Holland & Landrum, 2021; Liang, Polvani, & Mitevski, 2022).

Accompanying with this amplified Arctic warming, Arctic precipitation is also projected to increase in the 21st century (Bintanja & Andry, 2017; Bintanja & Selten, 2014; McCrystall et al., 2021; Vihma et al., 2016) and become more extreme (Landrum & Holland, 2020). This precipitation increase is conventionally attributed to an increase in moisture supply owing to the substantial retreat of sea ice and the resultant increase in open water (Bintanja & Selten, 2014; Boisvert & Stroeve, 2015; Serreze et al., 2012; Vihma et al., 2016), stronger poleward moisture transport (Woods et al., 2013; Zhang et al., 2013), and higher atmospheric temperatures that enable the atmosphere to contain more moisture (Bintanja, 2018; Screen & Simmonds, 2010). A recent study proposed another theory suggesting that the precipitation increase is constrained by atmospheric radiative cooling, particularly in regions covered by sea ice (Pithan & Jung, 2021). However, these studies did not specifically investigate seasonal shifts in precipitation, which are expected to correspond to the seasonal shifts in Arctic temperature and SIA loss.

By applying the uncertainty decomposition framework synthesized by Lehner et al. (2020), several studies have decomposed the total uncertainty in climate model projections into components associated with model structural differences, emission scenarios, and internal variability and have analyzed their temporal evolutions and relative importance over the course of the 21st century. For the Arctic specifically, Bonan et al. (2021) analyzed changes in SIA and found that by the end of the 21st century, scenario uncertainty dominates the uncertainty in summertime SIA loss, whereas model structural uncertainty primarily contributes to the uncertainty in wintertime SIA loss. Cai et al. (2021) employed a similar framework to decompose the uncertainty in 21st century Arctic warming and demonstrated that model uncertainty mainly affects the Arctic Ocean and land fields. More recently, Ono et al. (2022) used a single climate model with various forcing scenarios and reported that the strength of AA is highly dependent on the scenario. However, these studies have investigated either in the annual mean sense or in specific months or seasons, thus precluding any assessment of the aforementioned seasonal shifts in Arctic climate change; moreover, most of them have not examined AA per se.

In this study, we extend the results of Liang, Polvani, and Mitevski (2022) and use multiple single-model initial-condition large ensembles (SMILEs) of model simulations. We first reproduce the results for Arctic warming and SIA loss presented by Bonan et al. (2021) and Holland and Landrum (2021), respectively, and then add new analyses of Arctic precipitation, THFs, and, in particular, AA. Instead of focusing only on annual mean values solely, we examine the full seasonal structure and evolution of projected 21st-century Arctic climate change and address the underlying mechanisms. Next, we apply SMILEs, in addition to the scenario simulations of CMIP Phase 5 (CMIP5), to perform an uncertainty decomposition analysis to compare the various models, different scenarios, and internal variability in terms of the seasonal evolution of AA. Finally, we discuss our results in the context of recent studies and highlight the influence of model structural uncertainty on projections of Arctic seasonality changes. A clear understanding of the sources of uncertainty in projections of Arctic climate and seasonality changes can enable a more accurate assessment of seasonal peak shifts in high-latitude ecosystems, socioeconomics, and geopolitics.

2. Data and Methods

In this study, we use six SMILEs from the Multi-Model Large Ensemble Archive (MMLEA; Deser et al., 2020), namely the Community Earth System Model (CESM1-CAM5; Kay et al., 2015, 40 members), the Canadian Earth System Model (CanESM2; Kirchmeier-Young et al., 2017, 50 members), the Commonwealth Scientific and Industrial Research Organisation (CSIRO-Mk3.6.0; Jeffrey et al., 2013, 30 members), the Geophysical Fluid Dynamics Laboratory (GFDL-CM3; Sun et al., 2018, 20 members), the Geophysical Fluid Dynamics Laboratory Earth System Model (GFDL-ESM2M; Rodgers et al., 2015, 30 members), and the Max Planck Institute Earth System Model (MPI-ESM; Maher et al., 2019, 100 members). All of these SMILEs are forced with anthropogenic emissions in accordance with the RCP8.5 scenario.

In addition to these SMILEs, we analyze the outputs of 18 models that contributed to CMIP5 (K. E. Taylor et al., 2012). For these models, we consider all of the RCP2.6, RCP4.5, and RCP8.5 scenarios. Moreover, to assign the same weight to each model, we examine only one simulation per model per scenario, despite some

models providing multiple simulations. These models are listed in Table S1 of Supporting Information S1 and are also selected on the basis of the procedure described by Bonan et al. (2021).

We analyze the following variables: SAT, total precipitation (convective plus large-scale precipitation, hereafter referred to as precipitation), SIA, and surface THFs (latent plus sensible heat fluxes, with positive values indicating heat release from the ocean into the atmosphere). The response for these variables is calculated as the difference (Δ) between the mean over the target 30 yr periods (i.e., temporal chunks from 1951–1980 to 2071–2100) and the mean over the reference period 1951–1980. We choose 1951–1980 as the reference period because CanESM2 provides its historical integrations starting from 1951 in the MMLEA. To test the robustness of these results, we repeat our analysis using different reference periods (e.g., 1921–1950), obtaining largely similar results (not shown).

Throughout the manuscript, the Arctic-averaged value indicates the latitude-weighted spatial average over the 70°N–90°N domain, whereas the global-averaged value spans the 90°S–90°N domain. We mask out grid points over land when calculating area-averaged sea-ice loss and the resultant THF change; nevertheless, we obtain similar results without land masking because, as expected, the THF change is much larger over oceans than it is over land.

To identify the mechanisms driving changes in Arctic precipitation and Arctic near-surface temperature changes, we compute the vertically integrated moisture budget and the top-of-atmosphere energy budget. The methodology details can be found in the Supporting Information.

We quantify AA by using an AA factor (hereafter AAF), which is expressed as follows:

$$AAF = \frac{\Delta T_{Arctic}}{\Delta T_{Global}}, \tag{1}$$

where ΔT_{Arctic} and ΔT_{Global} are the SAT changes in the 30 yr mean (Δ) in the Arctic and global domains, respectively. Some previous studies (e.g., Liang et al., 2022; Polvani et al., 2020) have calculated the AAF as the Arctic warming trend divided by the global warming trend. We attempt to calculate the AAF by using trends instead of epoch differences, but we obtain unreasonably large magnitude values in the RCP2.6 and RCP4.5 simulations in the late 21st century, when ΔT_{Global} is often close to zero. Ono et al. (2022) also used epoch differences instead of trends because they also obtained similar unreasonable results. Thus, in the subsequent sections, we present the AAF computed on the basis of the difference in 30 yr means.

Following Lehner et al. (2020), we decompose the total projection uncertainty U_T in AA and related climate changes into components associated with model structural uncertainty (hereafter U_M), emission scenario uncertainty (hereafter U_S), and internal variability (hereafter U_I):

$$U_T(t) = U_M(t) + U_S(t) + U_I(t), \tag{2}$$

where each component depends on time t. U_M is computed as the variance across six ensemble-mean SMILEs under RCP8.5 forcing and represents the model-to-model difference after the reduction of internal variability effects. We also find that the variables derived from the SMILEs and CMIP5 models are largely comparable under RCP8.5 forcing (cf. leftmost and rightmost columns in Figure S1 of Supporting Information S1), indicating that SMILEs represent the intermodel spread of CMIP5 models. The peaks of the CMIP5-RCP8.5 AAF do not have evident seasonal shifts; this may be due to the strong warming that inhibits AA (see Section 3 for the relevant discussion). U_S is computed as the variance across the CMIP5 multimodel means of the RCP2.6, RCP4.5, and RCP8.5 scenarios. Finally, U_I is computed as the mean of the variance across ensemble members in each SMILE. We apply this uncertainty decomposition framework for each month individually to analyze the seasonality changes. Figure 4 displays the variances for each decomposed uncertainty instead of the percentages presented in Bonan et al. (2021). To confirm that our calculation for uncertainty decomposition is correct, we also calculate the percentages and compare them with those of Bonan et al. (2021). We obtain largely similar results (not shown).

3. Results

We first examine the seasonal evolution of the ensemble-mean responses of Arctic precipitation, SAT, THF, and SIA across six SMILEs (Figure 1) to illustrate the underlying physical processes leading to seasonal differences

in Arctic climate change. The annual maxima (i.e., the maximum monthly values of each year, indicated by gray dots) reveal that the SAT and THF responses, except for those from GFDL-ESM2M, have consistent seasonal shifts from October–November in the early-to-middle 21st century to December–January in the late 21st century. The maxima of SAT and THF tend to lag the SIA shift by approximately 1 month; this phenomenon is evident in CESM1-CAM5, CanESM2, GFDL-CM3, and MPI-ESM but not in CSIRO-MK3.6.0 or GFDL-ESM2M. This suggests that a mechanism involving increased SIA loss later in autumn—accompanied by a seasonal shift in the maximum THF release from the ocean to the atmosphere—engenders the seasonal shift in SAT responses. Additionally, the SIA losses in some models (e.g., CanESM2 and GFDL-CM3) have secondary peaks in early summer, suggesting the "summer mode" identified in a previous study (Onarheim et al., 2018).

In addition to the seasonal shifts in SIA and THF responses, a similar shift might be expected in the Arctic precipitation response owing to the presence of a stronger local moisture source (i.e., enhanced surface evaporation) later in autumn due to SIA loss. This precipitation maximum shift does indeed occur in CESM1-CAM5, GFDL-ESM2M, and MPI-ESM but not in CanESM2 or GFDL-CM3. In CSIRO-Mk3.6.0, the annual maximum Arctic precipitation response shifts seasonally in the opposite direction over the 21st century, moving from October to September. Although the reasons for this qualitatively different response are unclear, we notice that the SIA loss in CSIRO-Mk3.6.0 (Figure 1u) is generally small (as reported in Bonan et al., 2021) and that its mean SIA is high (Jahn et al., 2016), leading to a delayed seasonal shift relative to the other models.

We next analyze the moisture and energy budgets over the Arctic domain to understand the mechanisms underlying the precipitation and SAT responses (Figures S2 and S3 in Supporting Information S1). We perform these

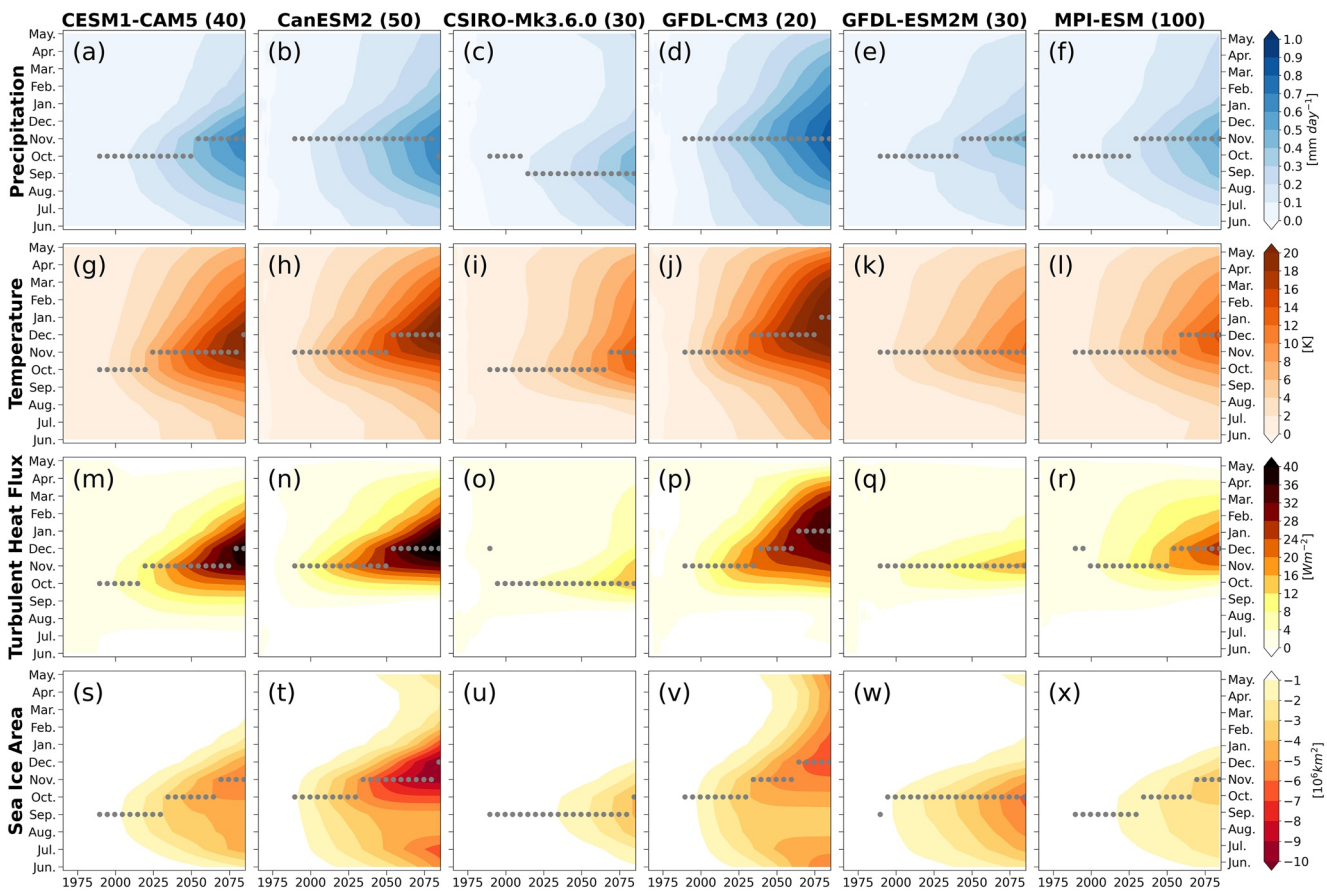

Figure 1. Seasonal evolution of (a–f) precipitation, (g–l) surface air temperature, (m–r) turbulent heat flux, and (s–x) sea-ice area responses, averaged over the Arctic domain (70°N–90°N) for six single-model initial-condition large ensembles (SMILEs) under RCP8.5 scenario. The responses are computed as the difference between the mean of a running 30 yr period and the mean of the 1951–1980 reference period; for each SMILE, the ensemble mean is shown. Years along the *x*-axis denote the centers of each 30 yr period, and the dots denote the annual maximum values, shown every 5 yr. The number of ensemble members in each SMILE is indicated in parentheses at the top.

analyses for only CESM1-CAM5 because of data availability. Our moisture budget analysis reveals that the surface latent heat fluxes are the dominant contributor to the precipitation seasonality changes; the annual maximum precipitation response shifts from October to November (cf., Figures S2a and S2d in Supporting Information S1). This is attributable to the greater open water area because SIA loss facilitates latent heat exchange between the ocean and atmosphere during autumn, consequently maximizing the increase in Arctic precipitation at this time of year. By contrast, the contributions of horizontal and vertical moisture advections are much smaller (Figures S2b and S2c in Supporting Information S1).

The energy budget analysis reveals that a similar mechanism is responsible for the seasonal shift in SAT response; this shift aligns well with a shift in the maximum oceanic heat release (ΔOHR, positive into the atmosphere) from October to November (Figure S3b in Supporting Information S1). Decomposing surface ΔOHR into latent and sensible heat fluxes and net longwave and shortwave radiations indicates that changes in THF indeed produce the SAT seasonal shift (Figure S3c in Supporting Information S1); neither shortwave nor longwave changes contribute significantly to the shift (not shown). The Planck and lapse-rate feedbacks also contribute to this SAT shift, although their individual contributions are smaller than that of the THF change (Figures S3g and S3h in Supporting Information S1). By contrast, the surface albedo (Figure S3f in Supporting Information S1) and water vapor feedbacks (Figure S3i in Supporting Information S1), which peak in summer, do not contribute directly to the seasonality changes during autumn and winter, although they can indirectly affect the lapse-rate feedback in winter (Feldl et al., 2020) and increase fall-winter conductive heat flux because of the delayed emergence of sea ice corresponding to reduced sea-ice thickness (SIT; Hahn et al., 2022; Landrum & Holland, 2022). In summary, our analysis suggests that a seasonal shift in SIA loss and associated changes in the turbulent heat exchange between the ocean and atmosphere is the key physical process leading to the seasonal shift in the SAT response, confirming the results of previous studies (Chung et al., 2021; Liang, Polvani, & Mitevski, 2022).

We next focus on the seasonality changes in AA. We quantify the strength of AA by using an AAF. Figures 2a–2f show that in the six SMILEs, the maximum AAF (gray dots) shifts from November to December over the course of the 21st century. This seasonal evolution is largely consistent with that of the Arctic SAT response (Figures 1g–1l), indicating that the seasonal shift in AA is dominated by seasonal changes in the Arctic (rather than global) SAT response. However, in contrast to the Arctic SAT response, which increases in magnitude monotonically throughout the 21st century, the AAF reaches its maximum between the 2000–2050 period and decreases thereafter. One reason for a weaker AA in the late 21st century is the saturation of the impact of SIA loss: the Arctic Ocean is nearly ice-free by this time in autumn/early winter, except in CSIRO-MK3.6.0; therefore, local feedback associated with SIA loss can no longer effectively amplify Arctic warming. Concurrently, increasing greenhouse gases continue to steadily warm the globe. These two factors combine to produce a smaller AAF, which has also been documented in previous studies (Chung et al., 2021; Deser et al., 2010; Liang, Polvani, & Mitevski, 2022).

An examination of different RCP forcing scenarios in CMIP5 (Figure 3) also shows that the maximum AAF exhibits a seasonal shift into winter as the forcing magnitude increases. Specifically, in 14 of 18 CMIP5 models, the annual maximum AAF shifts forward (i.e., later in the year) by 1 month in RCP8.5 relative to RCP2.6. This is consistent with the finding of another recent study, which also revealed that the AAF exhibits a seasonal shift in the high-SSP scenario in the CMIP6 model compared with the low-SSP scenario (see Figure S8 in Supporting Information S1 of Liang, Polvani, and Mitevski (2022)).

Although the maximum AAF is shown to shift in most individual models and in the multimodel mean (Figure 2g), we observe that the timing and magnitude of this shift exhibits a considerable spread across the models (see also Holland and Landrum (2021)). This spread is also indicated in Figure 2h, where the region of relatively small signal-to-noise ratios (blue dots) shifts from autumn into winter over the 21st century, implying a large inter-model spread owing to model-to-model difference in these seasons. This motivates us to decompose the total projection uncertainty for the AAF and the related climate variables into components associated with model uncertainty, emission scenario uncertainty, and internal variability, as defined in Section 2. Figure 4 displays the decomposition of the uncertainty magnitudes of the Arctic precipitation, SAT, AAF, and SIA responses over the 21st century. As indicated in the figure, the model structural uncertainty U_M explains the majority of the total fall-winter uncertainty U_T, with both U_M and U_T exhibiting highly similar seasonal shifts in their maxima for all variables (cf. first and second columns of Figure 2). Much of the model (and thus total) uncertainty in projections of precipitation, SAT, and AAF stems from model-to-model differences in projected SIA loss, considering the

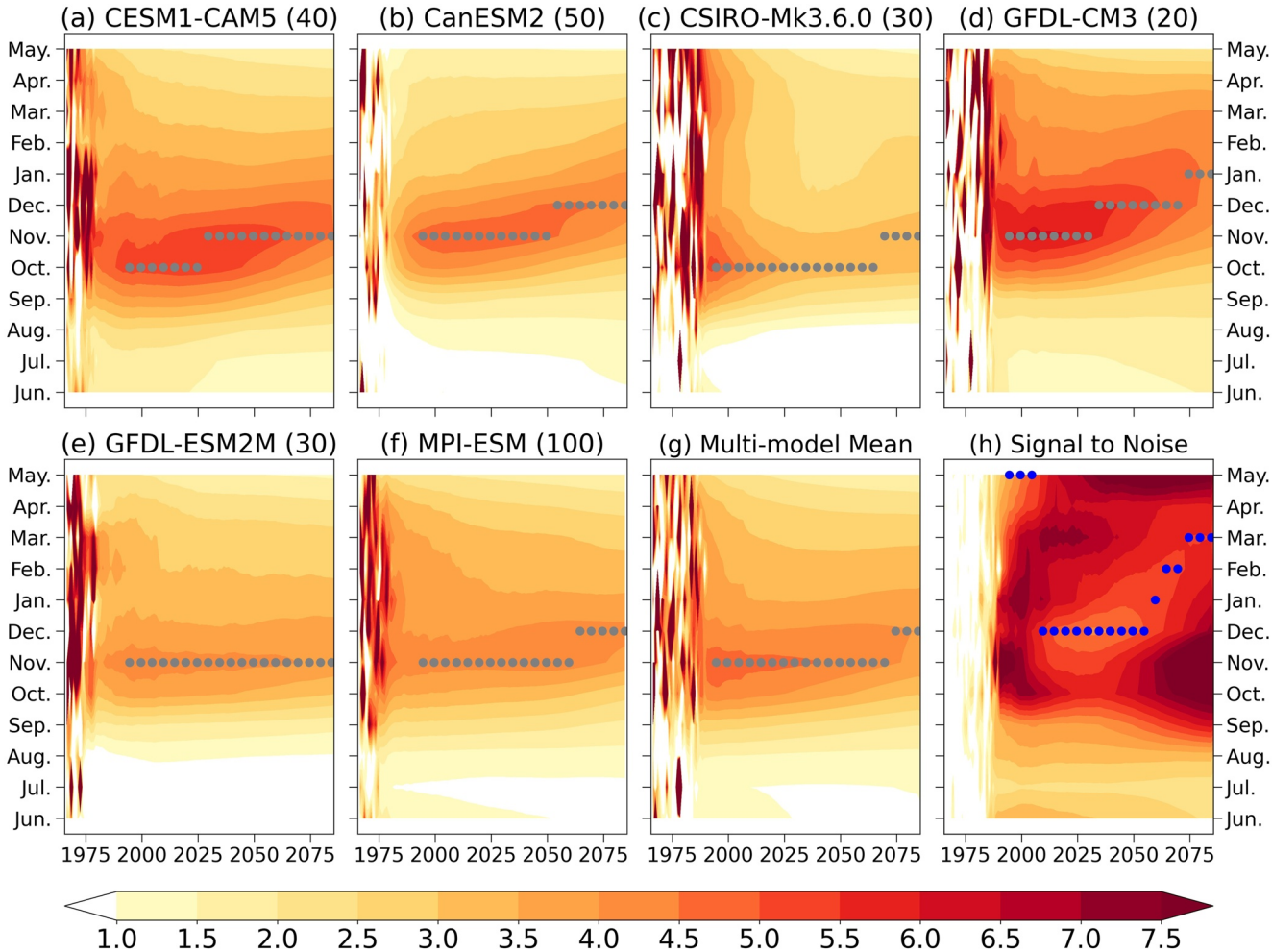

Figure 2. Seasonal evolution of the AAF in (a–f) six single-model initial-condition large ensembles (SMILEs) with RCP8.5 forcing and (g) the multi-SMILE mean across six models. Panel (h) displays the signal-to-noise ratio, defined as the ratio of the multi-SMILE mean to the multi-SMILE standard deviation. Years along the *x*-axis denote the centers of each 30 yr period, gray dots in (a–f) denote the annual maximum AAF every 5 yr, and blue dots in (h) denote the annual minimum signal-to-noise ratio of the AAF every 5 yr from October to May. Values in parentheses in the titles of (a–f) indicate the number of ensemble members in each SMILE.

dominant role of SIA loss in shaping these other climate responses, as discussed earlier. For the precipitation, SAT, and SIA, both U_M and U_T increase over the 21st century along with the increase in the mean responses for these variables. By contrast, for the AAF, the maxima of U_M and U_T occur during the first half of the century (particularly in late autumn/early winter), and both decrease thereafter. This temporal evolution of uncertainty once again follows that of the AAF mean (Figure 2). Notably, the result of the uncertainty decomposition for SIA (Figures 4m–4p), showing that U_M dominates over U_S even in summer, is different from the conclusion drawn by Bonan et al. (2021). This inconsistency is attributed to the difference in the chosen time-window length (30 vs. 5 yr) and difference in definition of uncertainty (variance vs. percentage) between the two studies.

U_S and U_I (cf. third and fourth columns of Figure 4) generally have a considerably smaller contribution to the total uncertainty than U_M does, and they do not have clear seasonal shifts. However, at the end of the 21st century, we find that U_S has a larger contribution to the total uncertainty in Arctic precipitation, SAT, and SIA responses relative to its contribution to the total uncertainty in the AAF. In the annual mean (Figures S4e, S4f, and S4h in Supporting Information S1), this contribution amounts to approximately 30%–40% of U_T. By contrast, the contribution of U_S to the total uncertainty in the AAF is much smaller (approximately 5% at the end of the 21st century; see Figure S4g in Supporting Information S1). Two reasons may explain this smaller contribution. First, the mean AAF is smaller at the end of the 21st century (Figure 2), with corresponding reductions in all sources of uncertainty (including U_S). Second, U_S for the Arctic SAT response is proportionally similar to that for the global

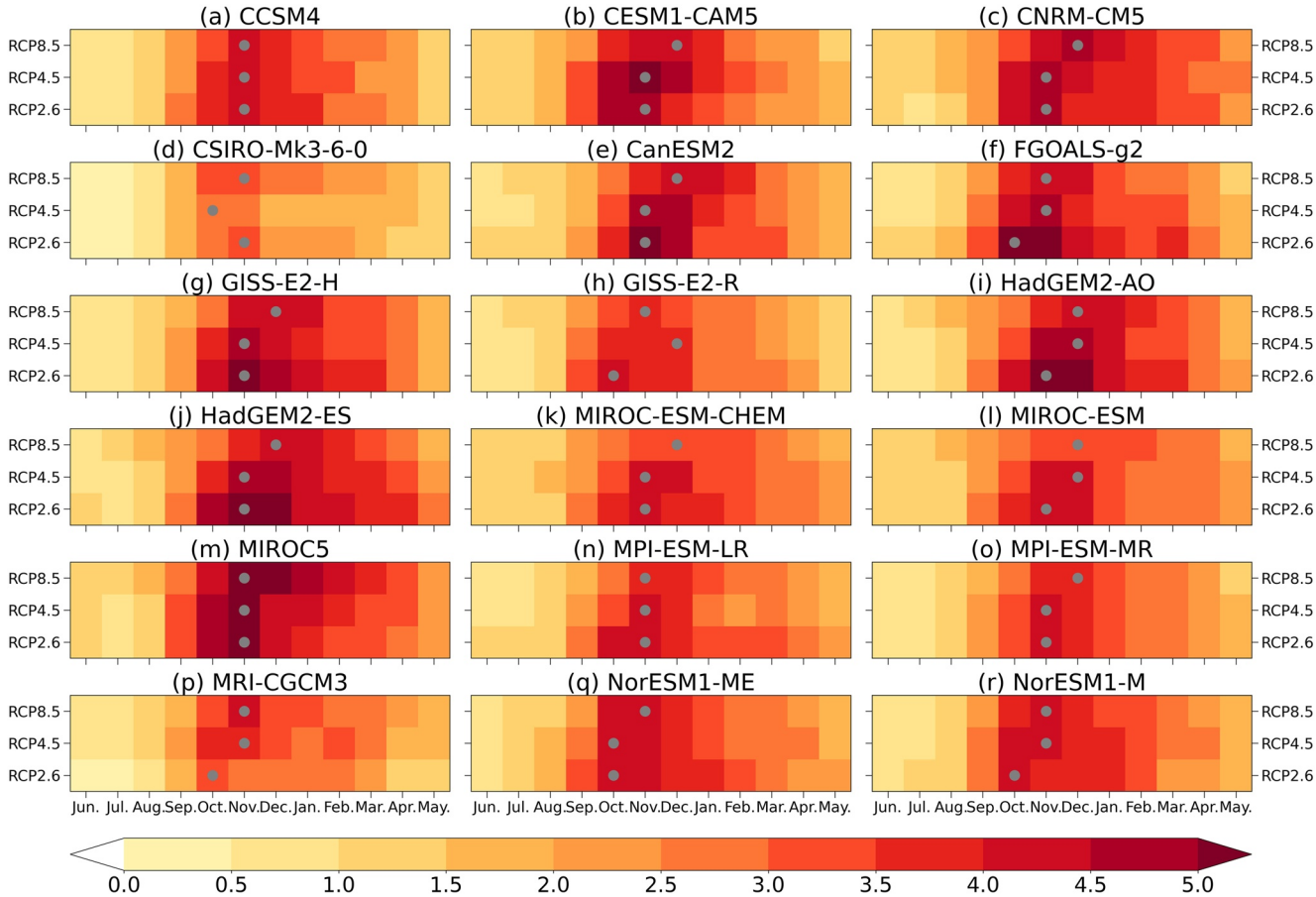

Figure 3. AAF for each month across 18 CMIP5 models at the end of the 21st century (2071–2100) in the RCP2.6, RCP4.5, and RCP8.5 scenarios. The reference period is 1951–1980, as for the single-model initial-condition large ensembles. Gray dots in each panel denote the maximum AAF value across 12 months.

SAT response, which can be manifested as the temporal evolution of their variance ratio (Figure S5c in Supporting Information S1). Because the AAF is defined as the ratio of Arctic and global SAT responses (see Methods), this could result in a relatively small contribution of U_S to the AAF uncertainty.

4. Discussion and Concluding Remarks

Recent studies have documented the seasonal shift in Arctic warming, the maximum value of which shifts from autumn into winter as a consequence of the increasing greenhouse gases forcing (Holland & Landrum, 2021; Liang, Polvani, & Mitevski, 2022) and changes in sea-ice heat capacity (Hahn et al., 2022). To extend these findings, we examine the seasonal evolution of Arctic SIA loss, surface THF, precipitation, SAT, and AA to determine the underlying mechanisms and analyze future projection uncertainties using 6 SMILEs and 18 CMIP5 scenario simulations. Our results confirm that the maximum Arctic SATs exhibit clear seasonal shifts toward boreal winter along with the corresponding seasonal shifts in SIA loss and THF release in the course of the 21st century. As expected, because Arctic warming dominates the AA signal, the annual peak of the AAF has a similar seasonal shift from autumn into winter. The amplitude of the AAF decreases with time; this phenomenon can largely be explained by the saturation of SIA loss, preventing sea-ice-related feedback from further enhancing existing warming (Chung et al., 2021; Deser et al., 2010; Holland & Landrum, 2021). SIA loss, therefore, plays a key role in regulating the seasonal evolution of Arctic climate change.

AA seasonality may be influenced by other mechanisms, particularly the Planck feedback and lapse-rate feedback, which were demonstrated to substantially affect the generation of AA during winter (Pithan & Mauritsen, 2014). However, our energy budget analysis indicates that they are less important than SIA-loss-related THF release into the atmosphere in terms of the strength, and the months in which they exhibit that the shifts are not consistent

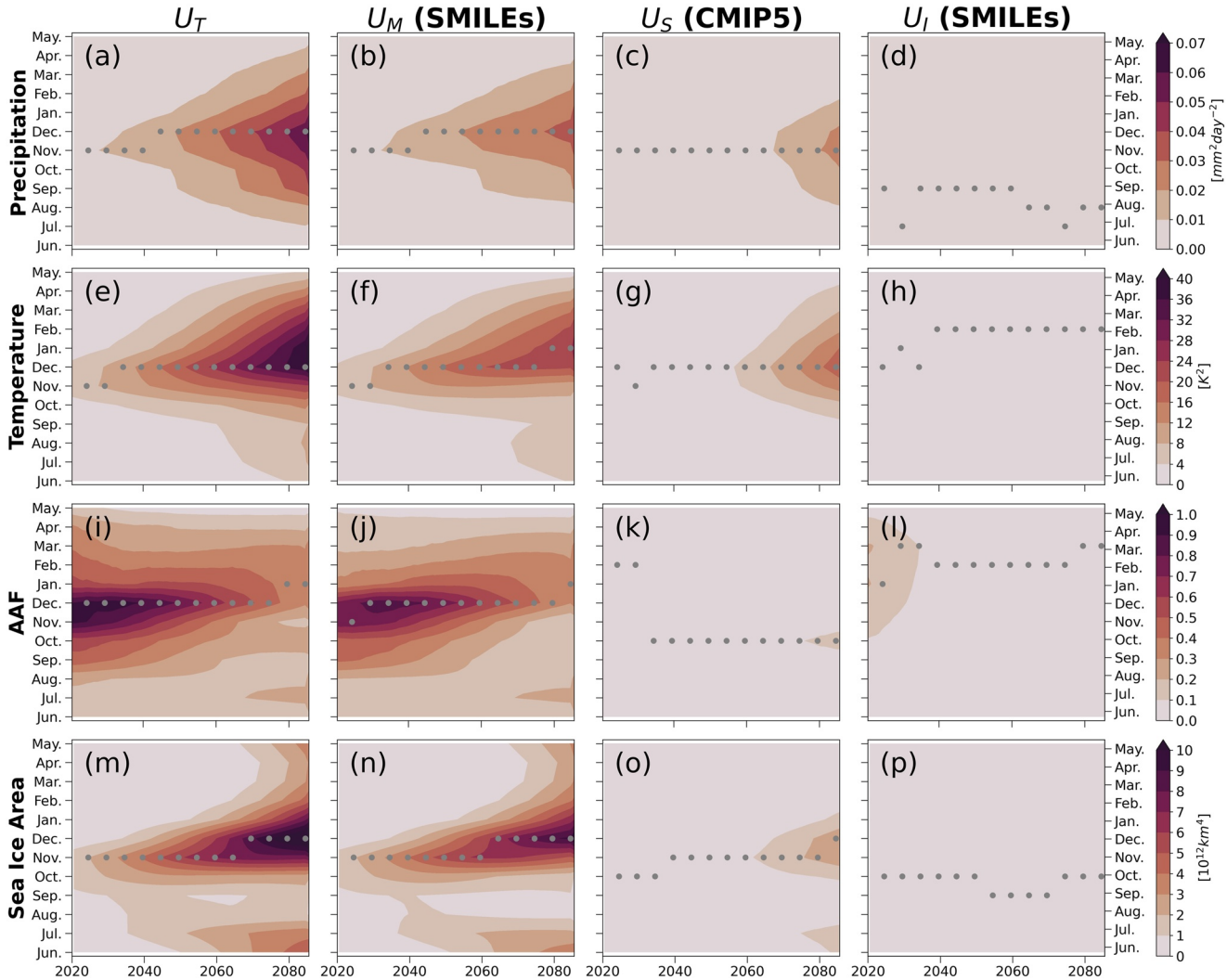

Figure 4. Seasonal evolution of uncertainty in projections of Arctic precipitation: (a) total uncertainty U_T, (b) model structural uncertainty U_M, (c) emission scenario uncertainty U_S, and (d) uncertainty due to internal variability U_I. (e–h) As in (a–d), but for Arctic surface air temperature response. (i–l) As in (a–d), but for the AAF. (m–p) As in (a–d), but for Arctic sea-ice area response. Years along the *x*-axis denote the centers of each 30 yr period, and gray dots denote the annual maximum values every 5 yr.

with those of THF. These results again support the key role of SIA loss in modulating wintertime Arctic climate seasonality and confirm the conclusions of previous studies (Dai et al., 2019; Feldl et al., 2020; Hahn et al., 2022; Jenkins & Dai, 2021; Liang, Polvani, & Mitevski, 2022). The sea-ice albedo feedback, although peaking in summer and not directly affecting the AA seasonal shift, could indirectly enhance both the lapse-rate feedback in winter (Feldl et al., 2020) and the sea-ice insulation feedback. However, these results should be used with caution because our feedback analysis is performed using only the CESM1-CAM5 model owing to data availability. A similar analysis with other models is warranted to assess the robustness of our findings.

A recent study highlighted the contribution of SIT change to Arctic warming (Landrum & Holland, 2022), which could also modulate the seasonality of warming peak. We examine the seasonal evolution of SIT for six SMILEs (Figure S6 in Supporting Information S1) and observe that changes in SIT may affect AA seasonality. We also observe that for some years, wintertime THF increases significantly, but SIA remains unchanged or exhibits only a small decrease (Figure 1). These THF increases, by contrast, coincide with thinning sea ice (Figure S6 in Supporting Information S1). This effect of SIT is consistent with the findings of Hahn et al. (2022), who suggested that the sea-ice capacity effect due to changes in SIT contributes to the seasonal shift in Arctic warming. Furthermore, the mean sea-ice state in a climate model could be crucial for determining Arctic climate

change (Previdi et al., 2021) and the timing and strength of climate shifts. For example, as reported by Bonan et al. (2021), CSIRO-Mk3.6.0 simulates excessive sea ice during the 21st century (Figure 1u), limiting the shifting months into winter or even delaying the shift to the end of this century. Further research is warranted to explore these aspects of SIT and model mean states.

We also find that the seasonal shift in the annual peaks of Arctic precipitation is not evident in CanESM2, CSIRO-Mk3.6.0, and GFDL-CM3 (Figures 1b–1d). This can be attributed to the excessively high mean sea-ice state in CSIRO-Mk3.6.0 (Figure S4d in Supporting Information S1), resulting in less open water and a smaller moisture source. However, this explanation does not seem plausible for CanESM2 and GFDL-CM3 because their SIAs are the smallest among the six SMILEs (Figure S4d in Supporting Information S1). Pithan and Jung (2021) proposed energy-constraint and moisture-constraint mechanisms driving Arctic precipitation change (see their Figure 4). Accordingly, we speculate that these mechanisms in the models may be not simulated well, leading to discrepancies in the seasonal shifts of precipitation. However, the relative importance (and sensitivity) of the energy-constrained and moisture-constrained precipitation in these models is unclear and requires further investigation.

In addition to investigating the seasonal shift in AA, our study is the first to apply the uncertainty decomposition framework of Lehner et al. (2020) to the monthly AAF. A key finding of our study is that unlike the uncertainty in global mean SAT projections, which is dominated by emission scenarios in the late 21st century (Figure S5b in Supporting Information S1), the uncertainty in the projection of AA is dominated by model structural differences, and scenario uncertainty plays a relative smaller role. Moreover, unlike the uncertainty in SAT or precipitation, the uncertainty in the AAF is greatest in the mid-21st century and declines afterward. We also observe that the scenario uncertainty for AAF is much lower than for the other variables. We attribute this finding to the intrinsic nature of AA, which is dependent on the relative warming of the Arctic compared with the whole globe.

Lastly, Ono et al. (2022) demonstrated that the strength of AA is dependent on the applied scenario, suggesting the importance of scenario uncertainty for AA projection. Moreover, in their study, results obtained from different models revealed this scenario dependence (Figure S16b in Supporting Information S1 of Ono et al. (2022)), but their multimodel spread (the rightmost error bars) is similar or even larger than the difference between two scenarios (i.e., the difference between blue and red dots). This implies that model-to-model differences could be comparable to the scenario uncertainty. Finally, we obtain our results regarding scenario uncertainty from only three CMIP5 scenario simulations. Future research should use additional models, ensembles, and scenario simulations from CMIP6 models to confirm the robustness of our results and reconcile our findings and those of Ono et al. (2022).

Data Availability Statement

The SMILEs were obtained from the MMLEA website (https://www.cesm.ucar.edu/community-projects/mmlea). The CMIP5 RCP simulations were downloaded from the World Climate Research Programme repository (https://esgf-node.llnl.gov/projects/cmip5/). The radiative kernel for CESM1 large ensemble was obtained from Dr. Angeline G. Pendergrass's Zenodo repository (https://zenodo.org/record/997902). The Python scripts for processing data and plotting figures are available on Y.-T. Wu's Zenodo repository (https://doi.org/10.5281/zenodo.6965473).

Acknowledgments
Y.-T. Wu and Y.-C. Liang are supported by grants from the Ministry of Science and Technology (111-2813-C-002-268-M, 110-2111-M-002-019-MY2 and 111-2628-M-002-011) to National Taiwan University. F. Lehner was supported by the Department of Energy (DE-SC0022070) and National Science Foundation (NSF IA, 1947282). L. M. Polvani was supported by a grant from NSF to Columbia University (1914569).

References

Bintanja, R. (2018). The impact of Arctic warming on increased rainfall. *Scientific Reports*, *8*(1), 1–6. https://doi.org/10.1038/s41598-018-34450-3
Bintanja, R., & Andry, O. (2017). Toward a rain-dominated Arctic. *Nature Climate Change*, *7*(4), 263–267. https://doi.org/10.1038/nclimate3240
Bintanja, R., & Selten, F. (2014). Future increases in Arctic precipitation linked to local evaporation and sea-ice retreat. *Nature*, *509*(7501), 479–482. https://doi.org/10.1038/nature13259
Boeke, R. C., & Taylor, P. C. (2018). Seasonal energy exchange in sea ice retreat regions contributes to differences in projected Arctic warming. *Nature Communications*, *9*(1), 1–14. https://doi.org/10.1038/s41467-018-07061-9
Boisvert, L., & Stroeve, J. C. (2015). The Arctic is becoming warmer and wetter as revealed by the atmospheric infrared sounder. *Geophysical Research Letters*, *42*(11), 4439–4446. https://doi.org/10.1002/2015gl063775
Bonan, D. B., Lehner, F., & Holland, M. M. (2021). Partitioning uncertainty in projections of Arctic sea ice. *Environmental Research Letters*, *16*(4), 044002. https://doi.org/10.1088/1748-9326/abe0ec
Cai, Z., You, Q., Wu, F., Chen, H. W., Chen, D., & Cohen, J. (2021). Arctic warming revealed by multiple CMIP6 models: Evaluation of historical simulations and quantification of future projection uncertainties. *Journal of Climate*, *34*(12), 4871–4892. https://doi.org/10.1175/jcli-d-20-0791.1

Chung, E.-S., Ha, K.-J., Timmermann, A., Stuecker, M. F., Bodai, T., & Lee, S.-K. (2021). Cold-season Arctic amplification driven by Arctic Ocean-mediated seasonal energy transfer. *Earth's Future*, *9*(2), e2020EF001898. https://doi.org/10.1029/2020ef001898

Chylek, P., Folland, C., Klett, J. D., Wang, M., Hengartner, N., Lesins, G., & Dubey, M. K. (2022). Annual mean Arctic amplification 1970–2020: Observed and simulated by CMIP6 climate models. *Geophysical Research Letters*, *49*(13), e2022GL099371. https://doi.org/10.1029/2022gl099371

Dai, A., Luo, D., Song, M., & Liu, J. (2019). Arctic amplification is caused by sea-ice loss under increasing CO_2. *Nature Communications*, *10*(1), 1–13. https://doi.org/10.1038/s41467-018-07954-9

Deser, C., Lehner, F., Rodgers, K. B., Ault, T., Delworth, T. L., DiNezio, P. N., et al. (2020). Insights from Earth System Model initial-condition large ensembles and future prospects. *Nature Climate Change*, *10*(4), 277–286. https://doi.org/10.1038/s41558-020-0731-2

Deser, C., Tomas, R., Alexander, M., & Lawrence, D. (2010). The seasonal atmospheric response to projected Arctic sea ice loss in the late twenty-first century. *Journal of Climate*, *23*(2), 333–351. https://doi.org/10.1175/2009jcli3053.1

Feldl, N., Po-Chedley, S., Singh, H. K., Hay, S., & Kushner, P. J. (2020). Sea ice and atmospheric circulation shape the high-latitude lapse rate feedback. *npj Climate and Atmospheric Science*, *3*(1), 1–9. https://doi.org/10.1038/s41612-020-00146-7

Goosse, H., Kay, J. E., Armour, K. C., Bodas-Salcedo, A., Chepfer, H., Docquier, D., et al. (2018). Quantifying climate feedbacks in Polar Regions. *Nature Communications*, *9*(1), 1–13. https://doi.org/10.1038/s41467-018-04173-0

Hahn, L. C., Armour, K. C., Battisti, D. S., Eisenman, I., & Bitz, C. M. (2022). Seasonality in Arctic warming driven by sea ice effective heat capacity. *Journal of Climate*, *35*(5), 1629–1642. https://doi.org/10.1175/jcli-d-21-0626.1

Holland, M. M., & Bitz, C. M. (2003). Polar amplification of climate change in coupled models. *Climate Dynamic*s, *21*(3), 221–232. https://doi.org/10.1007/s00382-003-0332-6

Holland, M. M., & Landrum, L. (2021). The emergence and transient nature of Arctic amplification in coupled climate models. *Frontiers of Earth Science*, *9*, 764. https://doi.org/10.3389/feart.2021.719024

Jahn, A., Kay, J. E., Holland, M. M., & Hall, D. M. (2016). How predictable is the timing of a summer ice-free Arctic? *Geophysical Research Letters*, *43*(17), 9113–9120. https://doi.org/10.1002/2016gl070067

Jeffrey, S., Rotstayn, L., Collier, M., Dravitzki, S., Hamalainen, C., Moeseneder, C., et al. (2013). Australia's CMIP5 submission using the CSIRO-Mk3.6 model. *Australian Meteorological and Oceanographic*, *63*(1), 1–14. https://doi.org/10.22499/2.6301.001

Jenkins, M., & Dai, A. (2021). The impact of sea-ice loss on Arctic climate feedbacks and their role for Arctic amplification. *Geophysical Research Letters*, *48*(15), e2021GL094599. https://doi.org/10.1029/2021gl094599

Kay, J. E., Deser, C., Phillips, A., Mai, A., Hannay, C., Strand, G., et al. (2015). The community Earth System Model (CESM) large ensemble project: A community resource for studying climate change in the presence of internal climate variability. *Bulletin of the American Meteorological Society*, *96*(8), 1333–1349. https://doi.org/10.1175/bams-d-13-00255.1

Kirchmeier-Young, M. C., Zwiers, F. W., & Gillett, N. P. (2017). Attribution of extreme events in Arctic sea ice extent. *Journal of Climate*, *30*(2), 553–571. https://doi.org/10.1175/jcli-d-16-0412.1

Landrum, L. L., & Holland, M. M. (2020). Extremes become routine in an emerging new Arctic. *Nature Climate Change*, *10*(12), 1108–1115. https://doi.org/10.1038/s41558-020-0892-z

Landrum, L. L., & Holland, M. M. (2022). Influences of changing sea ice and snow thicknesses on simulated Arctic winter heat fluxes. *The Cryosphere*, *16*(4), 1483–1495. https://doi.org/10.5194/tc-16-1483-2022

Lehner, F., Deser, C., Maher, N., Marotzke, J., Fischer, E. M., Brunner, L., et al. (2020). Partitioning climate projection uncertainty with multiple large ensembles and CMIP5/6. *Earth System Dynamics*, *11*(2), 491–508. https://doi.org/10.5194/esd-11-491-2020

Liang, Y.-C., Polvani, L. M., & Mitevski, I. (2022). Arctic amplification, and its seasonal migration, over a wide range of abrupt CO_2 forcing. *npj Climate and Atmospheric Science*, *5*(1), 1–9. https://doi.org/10.1038/s41612-022-00228-8

Liang, Y.-C., Polvani, L. M., Previdi, M., Smith, K. L., England, M. R., & Chiodo, G. (2022). Stronger Arctic amplification from ozone-depleting substances than from carbon dioxide. *Environmental Research Letters*, *17*(2), 024010. https://doi.org/10.1088/1748-9326/ac4a31

Maher, N., Milinski, S., Suarez-Gutierrez, L., Botzet, M., Dobrynin, M., Kornblueh, L., et al. (2019). The max Planck Institute grand ensemble: Enabling the exploration of climate system variability. *Journal of Advances in Modeling Earth Systems*, *11*(7), 2050–2069. https://doi.org/10.1029/2019ms001639

Manabe, S., & Wetherald, R. T. (1975). The effects of doubling the CO_2 concentration on the climate of a general circulation model. *Journal of the Atmospheric Sciences*, *32*(1), 3–15. https://doi.org/10.1175/1520-0469(1975)032<0003:teodtc>2.0.co;2

McCrystall, M. R., Stroeve, J., Serreze, M., Forbes, B. C., & Screen, J. A. (2021). New climate models reveal faster and larger increases in Arctic precipitation than previously projected. *Nature Communications*, *12*(1), 1–12. https://doi.org/10.1038/s41467-021-27031-y

Onarheim, I. H., Eldevik, T., Smedsrud, L. H., & Stroeve, J. C. (2018). Seasonal and regional manifestation of Arctic sea ice loss. *Journal of Climate*, *31*(12), 4917–4932. https://doi.org/10.1175/jcli-d-17-0427.1

Ono, J., Watanabe, M., Komuro, Y., Tatebe, H., & Abe, M. (2022). Enhanced Arctic warming amplification revealed in a low-emission scenario. *Communications Earth & Environment*, *3*(1), 1–9. https://doi.org/10.1038/s43247-022-00354-4

Pithan, F., & Jung, T. (2021). Arctic amplification of precipitation changes—The energy hypothesis. *Geophysical Research Letters*, *48*(21), e2021GL094977. https://doi.org/10.1029/2021gl094977

Pithan, F., & Mauritsen, T. (2014). Arctic amplification dominated by temperature feedbacks in contemporary climate models. *Nature Geoscience*, *7*(3), 181–184. https://doi.org/10.1038/ngeo2071

Polvani, L. M., Previdi, M., England, M. R., Chiodo, G., & Smith, K. L. (2020). Substantial twentieth-century Arctic warming caused by ozone-depleting substances. *Nature Climate Change*, *10*(2), 130–133. https://doi.org/10.1038/s41558-019-0677-4

Previdi, M., Smith, K. L., & Polvani, L. M. (2021). Arctic amplification of climate change: A review of underlying mechanisms. *Environmental Research Letters*, *16*(9), 093003. https://doi.org/10.1088/1748-9326/ac1c29

Rantanen, M., Karpechko, A. Y., Lipponen, A., Nordling, K., Hyvärinen, O., Ruosteenoja, K., et al. (2022). The Arctic has warmed nearly four times faster than the globe since 1979. *Communications Earth & Environment*, *3*(1), 1–10. https://doi.org/10.1038/s43247-022-00498-3

Rodgers, K. B., Lin, J., & Frölicher, T. L. (2015). Emergence of multiple ocean ecosystem drivers in a large ensemble suite with an Earth System Model. *Biogeosciences*, *12*(11), 3301–3320. https://doi.org/10.5194/bg-12-3301-2015

Screen, J. A., & Simmonds, I. (2010). Increasing fall-winter energy loss from the Arctic Ocean and its role in Arctic temperature amplification. *Geophysical Research Letters*, *37*(16). https://doi.org/10.1029/2010gl044136

Sejas, S. A., Cai, M., Hu, A., Meehl, G. A., Washington, W., & Taylor, P. C. (2014). Individual feedback contributions to the seasonality of surface warming. *Journal of Climate*, *27*(14), 5653–5669. https://doi.org/10.1175/jcli-d-13-00658.1

Serreze, M. C., Barrett, A. P., & Stroeve, J. (2012). Recent changes in tropospheric water vapor over the Arctic as assessed from radiosondes and atmospheric reanalyses. *Journal of Geophysical Research: Atmospheres*, *117*(D10). https://doi.org/10.1029/2011jd017421

Sun, L., Alexander, M., & Deser, C. (2018). Evolution of the global coupled climate response to Arctic sea ice loss during 1990–2090 and its contribution to climate change. *Journal of Climate*, *31*(19), 7823–7843. https://doi.org/10.1175/jcli-d-18-0134.1

Taylor, K. E., Stouffer, R. J., & Meehl, G. A. (2012). An overview of CMIP5 and the experiment design. *Bulletin of the American Meteorological Society*, *93*(4), 485–498. https://doi.org/10.1175/bams-d-11-00094.1

Taylor, P. C., Boeke, R. C., Boisvert, L. N., Feldl, N., Henry, M., Huang, Y., et al. (2021). Process drivers, inter-model spread, and the path forward: A review of amplified Arctic warming. *Frontiers of Earth Science*, *9*(9). https://doi.org/10.3389/feart.2021.758361

Vihma, T., Screen, J., Tjernström, M., Newton, B., Zhang, X., Popova, V., et al. (2016). The atmospheric role in the Arctic water cycle: A review on processes, past and future changes, and their impacts. *Journal of Geophysical Research: Biogeosciences*, *121*(3), 586–620. https://doi.org/10.1002/2015jg003132

Woods, C., Caballero, R., & Svensson, G. (2013). Large-scale circulation associated with moisture intrusions into the Arctic during winter. *Geophysical Research Letters*, *40*(17), 4717–4721. https://doi.org/10.1002/grl.50912

Zhang, X., He, J., Zhang, J., Polyakov, I., Gerdes, R., Inoue, J., & Wu, P. (2013). Enhanced poleward moisture transport and amplified northern high-latitude wetting trend. *Nature Climate Change*, *3*(1), 47–51. https://doi.org/10.1038/nclimate1631

References From the Supporting Information

Chou, C., & Lan, C.-W. (2012). Changes in the annual range of precipitation under global warming. *Journal of Climat*e, *25*(1), 222–235. https://doi.org/10.1175/jcli-d-11-00097.1

Lan, C.-W., Lo, M.-H., Chou, C., & Kumar, S. (2016). Terrestrial water flux responses to global warming in tropical rainforest areas. *Earth's Future*, *4*(5), 210–224. https://doi.org/10.1002/2015ef000350

Liang, Y.-C., Lo, M.-H., Lan, C.-W., Seo, H., Ummenhofer, C. C., Yeager, S., et al. (2020). Amplified seasonal cycle in hydroclimate over the Amazon River basin and its plume region. *Nature Communications*, *11*(1), 1–11. https://doi.org/10.1038/s41467-020-18187-0

Pendergrass, A. G., Conley, A., & Vitt, F. M. (2018). Surface and top-of-atmosphere radiative feedback kernels for CESM-CAM5. *Earth System Science Data*, *10*(1), 317–324. https://doi.org/10.5194/essd-10-317-2018

Soden, B. J., Held, I. M., Colman, R., Shell, K. M., Kiehl, J. T., & Shields, C. A. (2008). Quantifying climate feedbacks using radiative kernels. *Journal of Climate*, *21*(14), 3504–3520. https://doi.org/10.1175/2007jcli2110.1